Influence of Pseudorange Accuracy on Phase Ambiguity Resolution in Various GPS Modernization Scenarios

Dennis Milbert, Ph.D.
Published: NAVIGATION, Spring 2005, 52(1), pp.29-38, by The Institute of Navigation
Revised: August 2005

ABSTRACT

A simulation of single epoch ambiguity resolution success rate under varying levels of pseudorange accuracy is conducted with a hypothetical, 12 satellite in view, GNSS configuration. Scenarios were run with no atmospheric error (short baseline), with ionosphere error, and with ionosphere and troposphere error contributions (long baseline). Additional calibrations and supporting model data were simulated by adding appropriate weights. The long baseline scenarios were extremely sensitive to the inclusion of ionosphere model data, and were also aided by the inclusion of troposphere data. When aided by such data, single epoch ambiguity resolution success rates of 95 to 97% were obtained with a 10 to 20 cm pseudorange RMS.

INTRODUCTION

The capability of measuring GNSS carrier phase and computing positions with centimeter-level accuracy is well established. However, the technology suffers in robustness due to the need to resolve the phase ambiguity in the computation process. For this reason, the successes of carrier phase positioning have been generally confined to static survey or short-baseline kinematic situations.

We are currently at the threshold of several technical advances driven by GPS modernization and by the deployment of the Galileo satellite system. In addition, certain instrumental and atmospheric propagation data sets, derived from GPS, are now being routinely generated. These advances are expected to have a significant impact on the carrier phase positioning problem.

A rich body of literature has been published which explores aspects of GPS modernization, Galileo deployment, and the application of propagation data to phase ambiguity resolution. Just a few examples are [1-3]. When considering the factors of three frequencies, two deployed constellations, and inclusion of ionospheric propagation data, it has been found that the inclusion of ionospheric data has the greatest impact on ambiguity resolution success rate.

One factor that has not received sufficient study in the literature is the influence of improved pseudorange accuracy on phase ambiguity resolution. Most papers adopt a set value for pseudorange accuracy. One exception is [4]. The authors consider

pseudorange accuracy in ambiguity resolution for the geometry-free case, where each satellite-receiver vector is treated independently. This represents a rather stringent situation. Geometry improvements from deployment of many satellites are not considered. In addition, that study did not encompass the inclusion of atmospheric propagation data.

The GPS pseudorange accuracy has improved over time. Crews [5] reports that the GPS user range error steadily decreased from 4.6 m RMS in 1990 to 1.5 m RMS in 2001. This improvement continues with a report of broadcast User Range Error of 1.1 m RMS in 2004 [6]. Further, early Galileo test bed experiments show pseudorange 95% accuracy (utilizing GPS Block IIR) of 45 cm, and one sigma, signal-in-space (no orbit or clock error) performance of 7 cm [7].

Given the technological advances in satellite clocks, denser global tracking networks, improved orbit and clock estimation in the control segments, deployment of the new signal modulations, advances in "smart" antennae that suppress multipath, and the potential of software receivers, it is increasingly important to consider pseudorange accuracy in the solution of the ambiguity resolution problem.

GENERAL METHODOLOGY

We setup a mathematical model which provides ambiguity resolution success rate, $P(\breve{z} = z)$, as a function of pseudorange accuracy, and when elaborated by a variety of other factors. The pseudorange, R, and the scaled carrier phase, $\Phi = \lambda\phi$, are measurements in units of meters. Only a single epoch case is considered. This provides a very conservative model, which is also robust against carrier phase cycle slips.

The satellite configuration is assumed to comprise 2 constellations (GPS and Galileo) that total 12 locally visible satellites. Two stations in Ohio gather the simulated data; COLB, the base station, and SIDN, a rover station, are separated by 103 km. The positions of the satellites are taken as the 8 that were actually visible shortly after 0 UTC on July 15, 2004. The remaining 4 simulated satellite positions were derived from 4 randomly selected GPS satellites that were not visible at the time. The simulated positions were computed by retaining the satellite-receiver vector azimuth and distance, and then by changing the sign of the vertical angle relative to the local geodetic horizon. This provided a convenient method to construct a single epoch scenario for hypothetical deployments some years in the future.

Following Odijk [3], the L1 pseudorange model is

$$R_j^l = \rho_j^l + dt_j - dt^l \qquad (1)$$

where

R_j^l L1 pseudorange from satellite l to receiver j (meters)

ρ_j^l geometric range from satellite *l* to receiver *j* (meters)

dt_j lumped bias parameter for receiver *j* (meters)

dt^l lumped bias parameter for satellite *l* (meters)

The notation is that subscripts denote a receiver index and that superscripts denote a satellite index. The index, *i*, denotes a single base receiver, *j* denotes a rover receiver, *k* denotes a single pivot satellite, and *l* denotes the 11 remaining non-pivot satellites. The lumped parameters contain both instrument bias as well as clock errors. Due to the rank defect noted in [3], these effects are combined. The lumping is not sufficient to remove all rank defects. So, a pivot satellite, *k*, is selected, and the bias term dt^k is omitted. Even though clock error is the dominant part of the bias parameters, they are scaled into units of meters. This gives the best conditioning of the linear system, and makes it easy to distinguish rank defects and weak geometries.

The pseudorange model yields a set of 4 equations expressing all possible combinations of base and rover receivers and pivot and non-pivot satellites,

$$\begin{aligned} R_i^k &= \rho_i^k + dt_i \\ R_i^l &= \rho_i^l + dt_i - dt^l \\ R_j^k &= \rho_j^k + dt_j \\ R_j^l &= \rho_j^l + dt_j - dt^l \end{aligned} \tag{2}$$

The L1 model for scaled carrier phase follows a novel setup of Goad [8],

$$\Phi_j^l = \rho_j^l + \lambda_1 M_j^l \tag{3}$$

where

λ_1 L1 wavelength (meters)

$M_j^l = N_j^l + \phi_j - \phi^l$ non-integer carrier ambiguity

and where

N_j^l integer phase ambiguity between satellite *l* and receiver *j*

ϕ_j fractional phase offset at receiver *j*

ϕ^l fractional phase offset at satellite *l*

The phase offsets express lumped parameters. They contain instrumental effects (including initial oscillator settings) as well as clock error. Rank defects prevent separation of these elements. In the Goad model, the set of phase equations explicitly formulate double difference (DD) integer ambiguities, N_{ij}^{kl}, between the base and rover receivers and the pivot and non-pivot satellites. Thus,

$$
\begin{aligned}
\Phi_i^k &= \rho_i^k + \lambda_1 M_i^k \\
\Phi_i^l &= \rho_i^l + \lambda_1 M_i^l \\
\Phi_j^k &= \rho_j^k + \lambda_1 M_j^k \\
\Phi_j^l &= \rho_j^l + \lambda_1 N_{ij}^{kl} + \lambda_1 M_j^k + \lambda_1 M_i^l - \lambda_1 M_i^k
\end{aligned}
\tag{4}
$$

where

$$
\begin{aligned}
N_{ij}^{kl} &= N_j^l - N_i^l - N_j^k + N_i^k \qquad \text{(integer)} \\
N_{ij}^{kl} &= M_j^l - M_i^l - M_j^k + M_i^k \qquad \text{(integer)}
\end{aligned}
$$

This setup allows retention of one-way (satellite-receiver) expressions while providing the capability to fix integer ambiguities. The one-way measurements may be treated as independent and uncorrelated. This avoids the need to handle the covariances generated by double differencing, while giving a rigorous solution.

Conceptually, a solution would be obtained by weighted least squares,

$$
(\boldsymbol{A}^t \boldsymbol{Q}^{-1} \boldsymbol{A})\, \boldsymbol{x} = \boldsymbol{A}^t \boldsymbol{Q}^{-1} \boldsymbol{y} \tag{5}
$$

with n observations and u unknown parameters, where

$\boldsymbol{A}$	matrix of observation equation partial differentials (n x u)
$\boldsymbol{Q}$	covariance matrix of observations (n x n)
$\boldsymbol{x}$	vector of unknown parameters (u x 1)
$\boldsymbol{y}$	vector of observations (n x 1)

The variance-covariance matrix of the unknowns is written,

$$
\boldsymbol{Q}_x = (\boldsymbol{A}^t \boldsymbol{Q}^{-1} \boldsymbol{A})^{-1} \tag{6}
$$

To avoid rank defects, partial derivatives of the geometric range are taken only for the rover coordinates. The base receiver coordinates are considered known. For the simple, L1-only, pseudorange and phase models (2) and (4), we have the unknown parameter set shown in Table 1.

Table 1 – Unknown Parameters, L1-only, Simple Model

Number of Unknowns (N--number of satellites)	Type
N-1	L1 integer DD carrier ambiguities
3	rover receiver position (XYZ)
2	pseudorange receiver lumped bias (base and rover)
N-1	pseudorange satellite lumped bias, non-pivot
1	L1 float ambiguity, pivot satellite to base
1	L1 float ambiguity, pivot satellite to rover
N-1	float ambiguity, non-pivot satellites to base

The system (5) is notable in that a subset of unknowns, the DD ambiguities, should be integer. The remaining unknowns will be real numbers. This creates a mixed integer, least squares problem. Teunessin [9] first described the LAMBDA method of solution of such a problem. Readers may recall the papers [10] and [11].

The system (5) is partitioned

$$\hat{\boldsymbol{x}} = \begin{bmatrix} \hat{\boldsymbol{a}} \\ \hat{\boldsymbol{b}} \end{bmatrix} \qquad \boldsymbol{Q}_{\hat{x}} = \begin{bmatrix} \boldsymbol{Q}_{\hat{a}} & \boldsymbol{Q}_{\hat{a}\hat{b}} \\ \boldsymbol{Q}_{\hat{b}\hat{a}} & \boldsymbol{Q}_{\hat{b}} \end{bmatrix} \tag{7}$$

where $\boldsymbol{a}$ denotes double difference ambiguities, $\boldsymbol{b}$ denotes remaining parameters, and where the ambiguity-float solution is marked by the "^" symbol. Inspection of $\boldsymbol{Q}_{\hat{a}}$ shows the float ambiguities are significantly correlated. LAMBDA computes a Gauss integer transformation, $\boldsymbol{Z}$, which decorrelates the covariance matrix, $\boldsymbol{Q}_{\hat{a}}$, as much as possible under certain requirements. $\boldsymbol{Z}$ must be computed such that transformed ambiguities, $\boldsymbol{z}=\boldsymbol{Z}^{\mathrm{t}}\boldsymbol{a}$, are integer, and that $\boldsymbol{Z}$ is regular. Thus, the elements of $\boldsymbol{Z}^{\mathrm{t}}$ and $\boldsymbol{Z}^{-\mathrm{t}}$ must be integer, while $\det(\boldsymbol{Z}^{\mathrm{t}})$ and $\det(\boldsymbol{Z}^{-\mathrm{t}})$ are ± 1. This approximate decorrelation is generally very effective, and allows highly efficient methods of integer ambiguity, $\breve{a}$, identification.

The LAMBDA method has been the object of much research, and has a large suite of statistical tools and results. Among them is a lower bound of the success rate of fixing *all* the ambiguities, a, to their correct integer values, $\breve{a}$. This conservative statistic [3,12] is

$$P(\breve{z} = z) \geq \prod_{i}^{n} \left[2G\left(\frac{1}{2\sigma^2_{\hat{z}_{i|I}}} \right) - 1 \right] \tag{8}$$

where the cumulative error function is

$$G(s) = \int_{-\infty}^{S} \frac{1}{\sqrt{2\pi}} \exp\left(-\frac{1}{2} t^2 \right) dt \tag{9}$$

$$G(-\infty) = 0 \qquad G(0) = 0.5 \qquad G(\infty) = 1$$

and where the conditional variances

$$\sigma^2_{\hat{z}_{i|I}} = \boldsymbol{D}(i,i) \tag{10}$$

are the diagonal elements of the decomposition

$$\boldsymbol{L}\boldsymbol{D}\boldsymbol{L}^t = \boldsymbol{Q}_{\hat{z}} \tag{11}$$

of the covariance matrix of the transformed float ambiguities

$$\boldsymbol{Q}_{\hat{z}} = \boldsymbol{Z}^t \boldsymbol{Q}_{\hat{a}} \boldsymbol{Z} \tag{12}$$

The success rate can be computed as a simulation, without any actual measurements, $\boldsymbol{y}$. One, of course, requires the partial derivatives, $\boldsymbol{A}$, for any model scenario. It is also worthy to note that the LAMBDA method is completely general, and can be applied to any mixed integer, least squares problem.

SHORT BASELINE SCENARIOS

These scenarios neglect ionosphere and troposphere model components. Such models are appropriate for baselines on the order of a few kilometers. In all cases, a one-way carrier phase accuracy of 3 mm RMS is adopted. The pseudorange RMS is allowed to vary from 5 mm to 1 m RMS. Pseudorange uses the model (2) and the carrier phase uses (4). The success rate (8) for fixing all 11 DD ambiguities is shown in Figure 1.

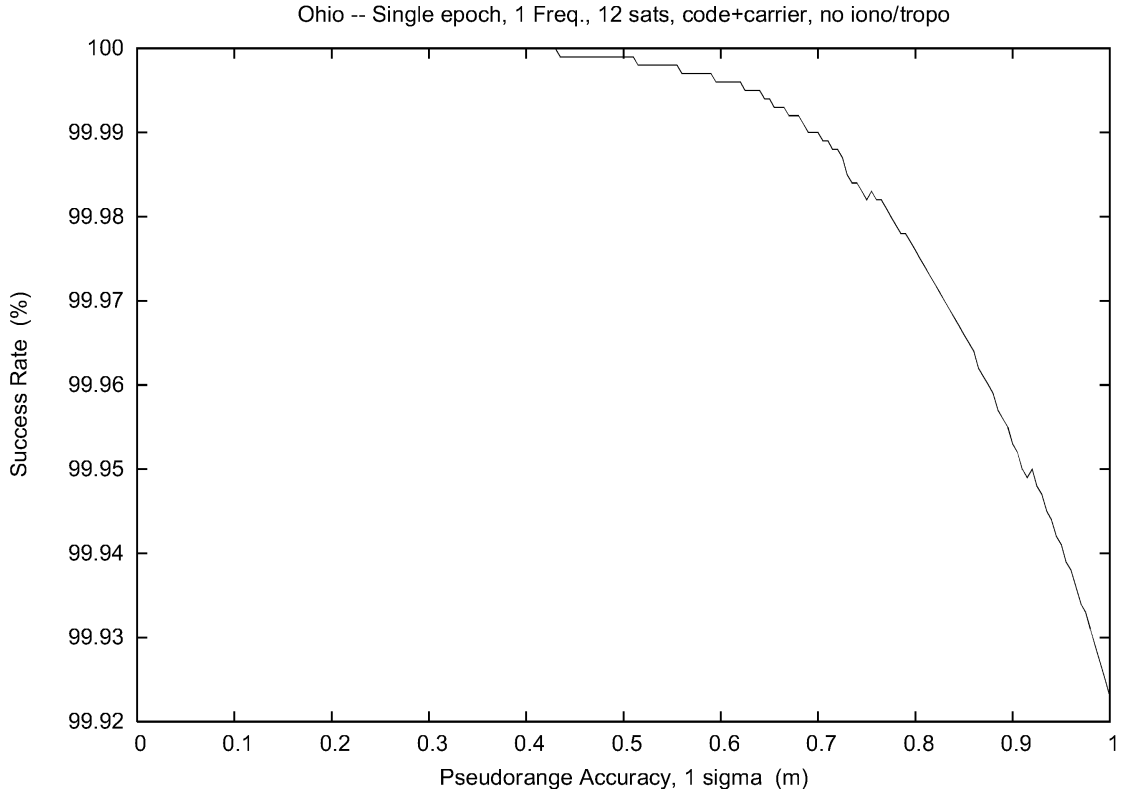

Fig 1. – Success Rate, L1-only, No Differential Ionosphere Effects

It is no surprise to see extremely high success rates, even with a 1 m RMS pseudorange. Commercial RTK equipment is available today that allows ambiguity resolution and centimeter-level positioning over short baselines.

We now require the L2 equation. It is realized that Galileo will not operate at L2 (1227.60 MHz), but at a nearby frequency, E5b (1207.14 MHz) [13]. For the purposes of this simulation, it can be considered close enough. For the L2 pseudoranges.

$$\begin{aligned} R_i^k &= \rho_i^k + D_i - D^k + dt_i \\ R_i^l &= \rho_i^l + D_i - D^l + dt_i - dt^l \\ R_j^k &= \rho_j^k + D_j - D^k + dt_j \\ R_j^l &= \rho_j^l + D_j - D^l + dt_j - dt^l \end{aligned} \tag{13}$$

where

D^k, D^l	satellite differential code bias (meters)
D_i, D_j	receiver differential code bias (meters)

Equations (13) differ from (2) by the inclusion of differential code bias (DCB). DCB is the difference between the L2 and the L1 instrumental errors that were previously lumped in the *dt* terms. DCB's are routinely computed for satellites and ground stations by the Center for Orbit Determination in Europe (CODE) [14-15].

The L2 carrier phase models are

$$\begin{aligned} \Phi_i^k &= \rho_i^k + \lambda_2 M_i^k \\ \Phi_i^l &= \rho_i^l + \lambda_2 M_i^l \\ \Phi_j^k &= \rho_j^k + \lambda_2 M_j^k \\ \Phi_j^l &= \rho_j^l + \lambda_2 N_{ij}^{kl} + \lambda_2 M_j^k + \lambda_2 M_i^l - \lambda_2 M_i^k \end{aligned} \tag{14}$$

The L2 *M* and *N* parameters are distinct from the L1 parameters. As described earlier, the *M*'s contain fractional phase offsets that include instrumental effects. Since the L2 *M* and *N* are distinct from the L1 *M* and *N*, there is no need to explicitly formulate differential carrier biases.

If (13) and (14) are added to the simulation, then a rank defect is encountered. It was confirmed by computing a singular value decomposition of the system (5). This weakness has the same characteristic as the one that forced the suppression of the dt^k terms in (2). Odijk [3] notes that as baselines grow shorter, and the satellite-receiver vectors become more parallel, such weaknesses will appear. Although only one defect is present, 12 satellite DCB constraints are added with 30-day CODE estimation RMS weights. The calibration of the satellite DCB's was applied with a 3 mm (about 10 ps) RMS accuracy. With the models (2,3,13,14), the success of fixing all 22 DD ambiguities is shown in Figure 2.

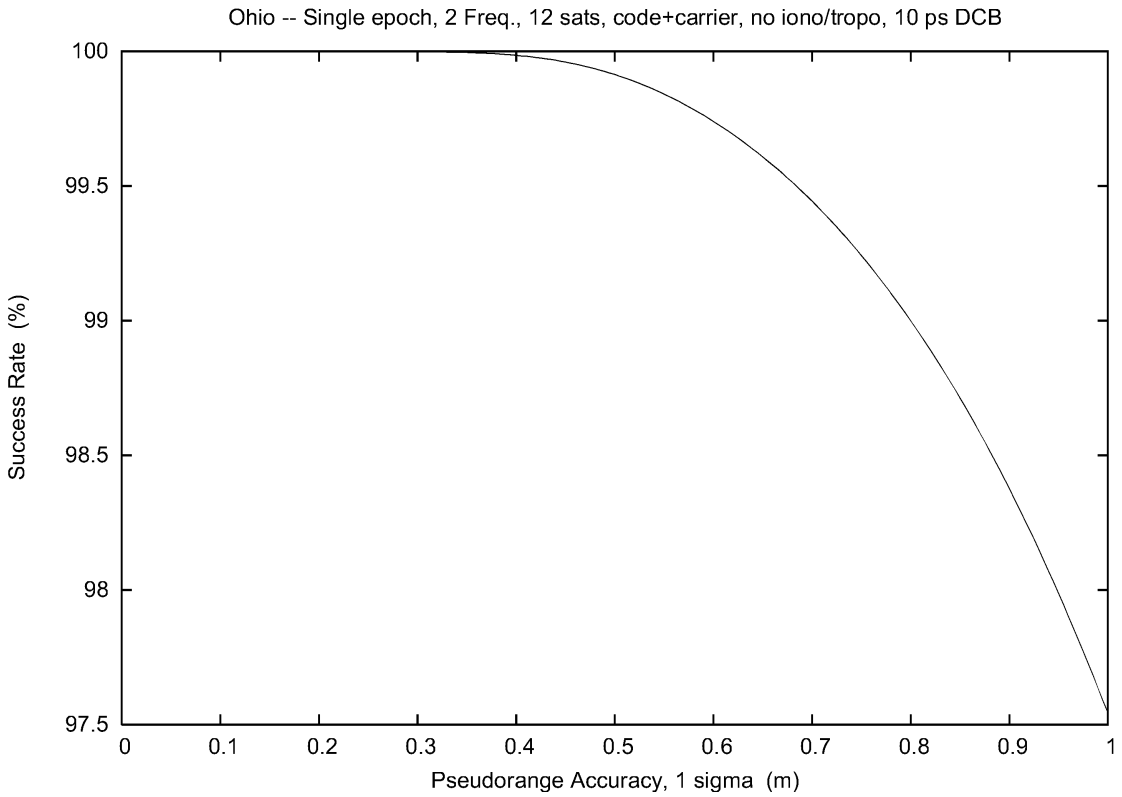

Fig 2. – Success Rate, L1/L2, No Differential Ionosphere Effects

Extremely high success rates are still obtained. The success is not as high with the L1-only case. The estimation of the additional DCB parameters, although weighted, mildly weakens the solution.

Next, L5 equations are written for range and phase,

$$\begin{aligned} R_i^k &= \rho_i^k + D_{5i} - D_5{}^k + dt_i \\ R_i^l &= \rho_i^l + D_{5i} - D_5{}^l + dt_i - dt^l \\ R_j^k &= \rho_j^k + D_{5_j} - D_5{}^k + dt_j \\ R_j^l &= \rho_j^l + D_{5_j} - D_5{}^l + dt_j - dt^l \end{aligned} \tag{15}$$

$$\begin{aligned} \Phi_i^k &= \rho_i^k + \lambda_5 M_i^k \\ \Phi_i^l &= \rho_i^l + \lambda_5 M_i^l \\ \Phi_j^k &= \rho_j^k + \lambda_5 M_j^k \\ \Phi_j^l &= \rho_j^l + \lambda_5 N_{ij}^{kl} + \lambda_5 M_j^k + \lambda_5 M_i^l - \lambda_5 M_i^k \end{aligned} \tag{16}$$

where

D_5^k, D_5^l satellite L1/L5 differential code bias (meters)
D_{5i}, D_{5j} receiver L1/L5 differential code bias (meters)

Equations (15) introduce new L5 DCB's, analogous to the regular L2 DCB's. It is assumed that calibration information will be available in the future, so the 12 satellite D_5 parameters are also weighted at 3 mm (about 10 ps) RMS accuracy. The L5 phase equations (16) contain non-integer and integer phase parameters that are analogous and distinct from the L2 parameters. The success rate for resolving all 33 DD ambiguities is displayed in Figure 3.

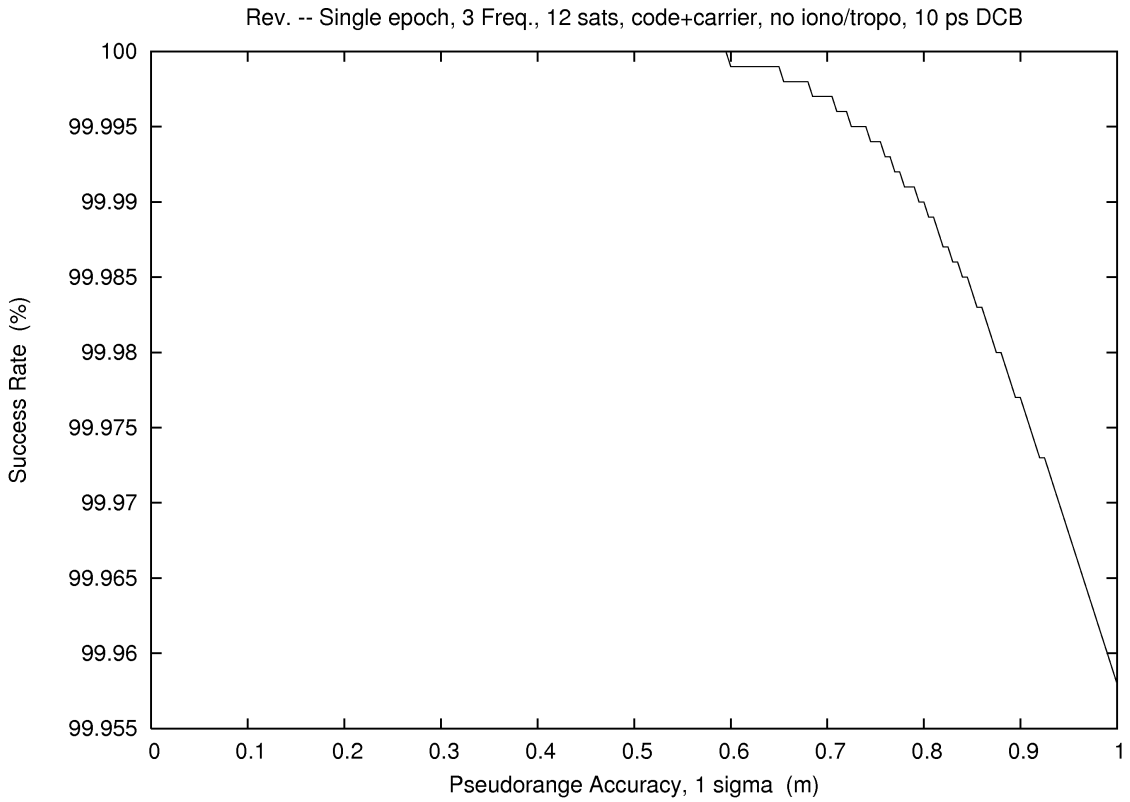

Fig 3. – Success Rate, L1/L2/L5, No Differential Ionosphere Effects

The triple frequency success rates are still extremely high, and fall between the single and dual frequency results. It is seen that adding the third frequency improves geometry, even when the 14 new L5 DCB's are added to the system.

IONOSPHERE ERROR SCENARIOS

The preceding results were characterized as "short baseline", since those are the only cases where atmospheric effects can be safely ignored. Ionosphere is parameterized in this section, and the troposphere will be parameterized in the subsequent section.

Ionosphere is modeled as distinct values for each satellite-receiver vector. Thus, no assumptions are made regarding azimuthal symmetry, nor about zenith delay mapping functions. The application of *a priori* ionosphere model data is anticipated. Therefore, following the methods used with the ambiguities, ionosphere is modeled as a combination of DD and un-differenced parameters. Unlike the ambiguities, there is no expectation that the DD ionosphere parameters will be integer. By this formulation, it is easy to apply both absolute and relative (i.e. DD) ionosphere model information. Also, it is convenient to express all ionospheric delays in units of meters on the L1 frequency.

For the L1 models,

$$\begin{aligned} R_i^k &= \rho_i^k + I_i^k + dt_i \\ R_i^l &= \rho_i^l + I_i^l + dt_i - dt^l \\ R_j^k &= \rho_j^k + I_j^k + dt_j \\ R_j^l &= \rho_j^l + I_{ij}^{kl} + I_j^k + I_i^l - I_i^k + dt_j - dt^l \end{aligned} \tag{17}$$

$$\begin{aligned} \Phi_i^k &= \rho_i^k - I_i^k + \lambda_1 M_i^k \\ \Phi_i^l &= \rho_i^l - I_i^l + \lambda_1 M_i^l \\ \Phi_j^k &= \rho_j^k - I_j^k + \lambda_1 M_j^k \\ \Phi_j^l &= \rho_j^l - I_{ij}^{kl} - I_j^k - I_i^l + I_i^k + \lambda_1 N_{ij}^{kl} + \lambda_1 M_j^k + \lambda_1 M_i^l - \lambda_1 M_i^k \end{aligned} \tag{18}$$

where

I_i^k	un-differenced ionosphere delay, pivot satellite to base (meters)
I_i^l	un-differenced ionosphere delay, non-pivot satellite to base (meters)
I_j^k	un-differenced ionosphere delay, pivot satellite to rover (meters)
I_{ij}^{kl}	double differenced ionosphere delay (meters)

For the L2 models,

$$\begin{aligned} R_i^k &= \rho_i^k + D_i - D^k + \mu_2 I_i^k + dt_i \\ R_i^l &= \rho_i^l + D_i - D^l + \mu_2 I_i^l + dt_i - dt^l \\ R_j^k &= \rho_j^k + D_j - D^k + \mu_2 I_j^k + dt_j \\ R_j^l &= \rho_j^l + D_j - D^l + \mu_2 I_{ij}^{kl} + \mu_2 I_j^k + \mu_2 I_i^l - \mu_2 I_i^k + dt_j - dt^l \end{aligned} \tag{19}$$

$$\begin{aligned} \Phi_i^k &= \rho_i^k - \mu_2 I_i^k + \lambda_2 M_i^k \\ \Phi_i^l &= \rho_i^l - \mu_2 I_i^l + \lambda_2 M_i^l \\ \Phi_j^k &= \rho_j^k - \mu_2 I_j^k + \lambda_2 M_j^k \\ \Phi_j^l &= \rho_j^l - \mu_2 I_{ij}^{kl} - \mu_2 I_j^k - \mu_2 I_i^l + \mu_2 I_i^k + \lambda_2 N_{ij}^{kl} + \lambda_2 M_j^k + \lambda_2 M_i^l - \lambda_2 M_i^k \end{aligned} \tag{20}$$

where the ionospheric delay on L2 is scaled to units of meters on L1 by,

$$\mu_2 = \left(\frac{\lambda_2}{\lambda_1}\right)^2$$

Two rank defects were identified after including the ionosphere unknowns. These weaknesses were remedied by introducing 2 DCB equations for the receivers, applied with a 33 mm (about 100 ps) RMS accuracy. The results for the dual frequency case with ionosphere estimation (but without external ionospheric data) and 14 DCB weights are shown in Figure 4.

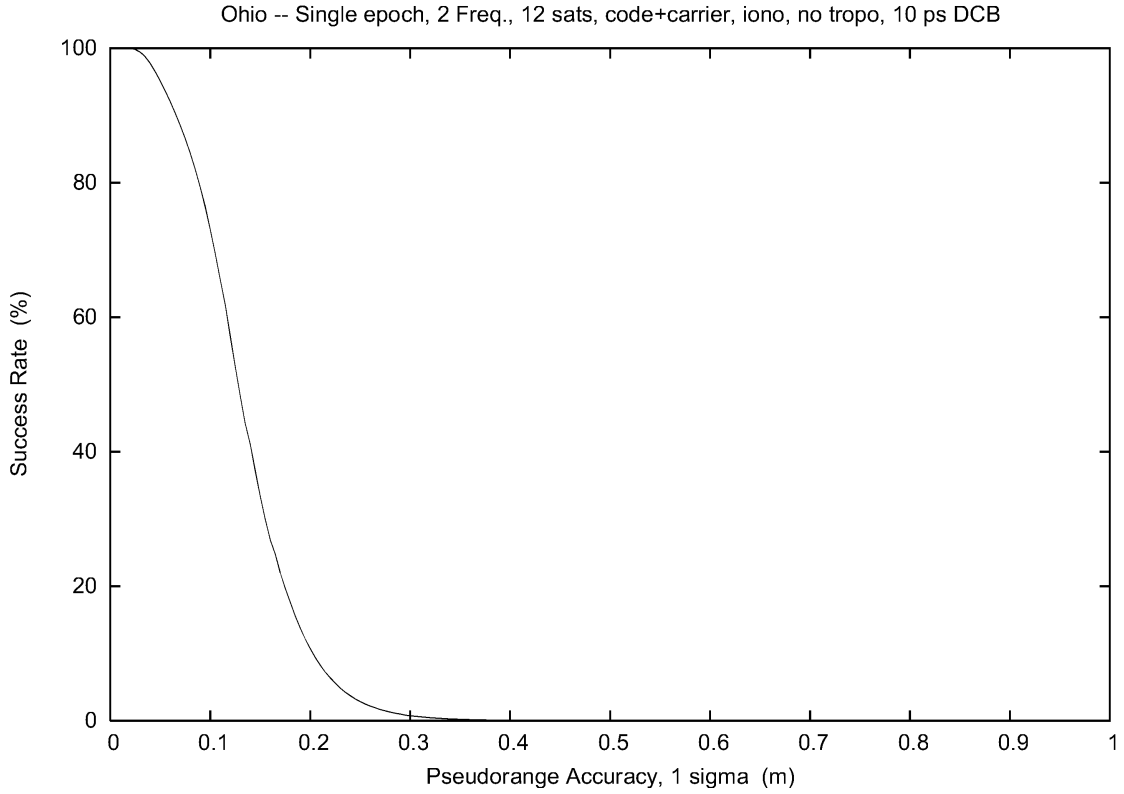

Fig 4. – Success Rate, L1/L2, with Ionosphere Parameters

A dramatic reduction in the success of fixing all 22 DD ambiguities is evident. This confirms the results by others (e.g. [2]) that ambiguity resolution success is closely related to ionospheric effects. Figure 4 also illustrates the importance of considering the achievable pseudorange accuracy in GPS modernization.

Next, the L5 models are extended to include ionosphere parameterization,

$$\begin{aligned} R_i^k &= \rho_i^k + D_{5i} - D_5^{\,k} + \mu_5 I_i^k + dt_i \\ R_i^l &= \rho_i^l + D_{5i} - D_5^{\,l} + \mu_5 I_i^l + dt_i - dt^l \end{aligned} \qquad (21)$$

$$
\begin{aligned}
R_j^k &= \rho_j^k + D_{5j} - D_5{}^k + \mu_5 I_j^k + dt_j \\
R_j^l &= \rho_j^l + D_{5j} - D_5{}^l + \mu_5 I_{ij}^{kl} + \mu_5 I_j^k + \mu_5 I_i^l - \mu_5 I_i^k + dt_j - dt^l \\
\\
\Phi_i^k &= \rho_i^k - \mu_5 I_i^k + \lambda_5 M_i^k \\
\Phi_i^l &= \rho_i^l - \mu_5 I_i^l + \lambda_5 M_i^l \\
\Phi_j^k &= \rho_j^k - \mu_5 I_j^k + \lambda_5 M_j^k \\
\Phi_j^l &= \rho_j^l - \mu_5 I_{ij}^{kl} - \mu_5 I_j^k - \mu_5 I_i^l + \mu_5 I_i^k + \lambda_5 N_{ij}^{kl} + \lambda_5 M_j^k + \lambda_5 M_i^l - \lambda_5 M_i^k
\end{aligned}
\tag{22}
$$

where the ionospheric delay on L5 is scaled to units of meters on L1 by,

$$\mu_5 = \left(\frac{\lambda_5}{\lambda_1}\right)^2$$

The success rates of fixing all 33 DD ambiguities for the triple frequency case are portrayed in Figure 5.

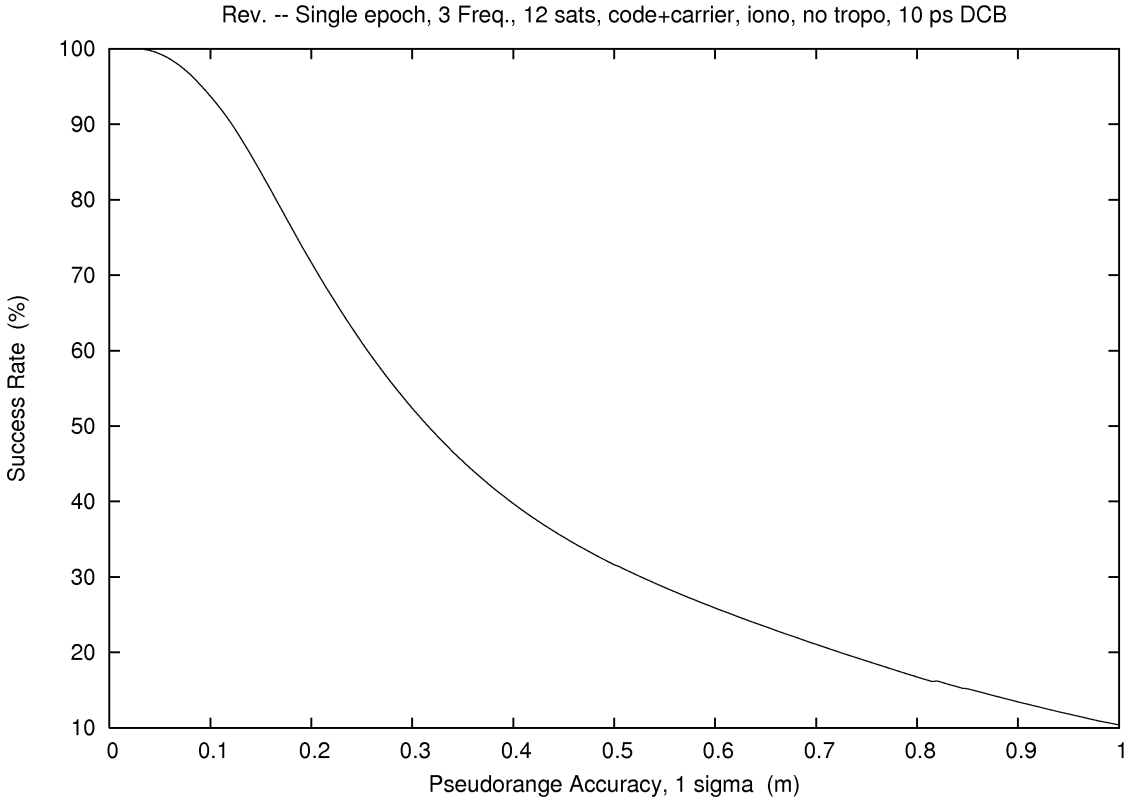

Fig 5. – Success Rate, L1/L2/L5, with Ionosphere Parameters

An improvement is seen when adding the third frequency. However, the improvement is modest. Recall the demanding context of single epoch ambiguity resolution.

Work by Odijk [2] and others illustrates that addition of ionospheric data (for example, from GPS monitor networks) has a great improvement of ambiguity resolution. The National Oceanic and Atmospheric Administration (NOAA) is now computing and distributing first-generation ionosphere models (see ftp://ftp.ngs.noaa.gov/cors/ionosphere/icon) which have crossover statistics of 0.5 Total Electron Content Unit (TECU) RMS and formal absolute error averaging 1.1 TECU (one sigma) [16]. While the current models suffer from track bias, it is expected that these precisions will be realizable as accuracies in the future. It seems reasonable to expect relative (DD) accuracy on L1 of 5 cm RMS and absolute accuracy on L1 of 15 cm RMS. The addition of 5 cm relative ionosphere weights is presented in Figure 6. And, the combination of 5 cm relative and 15 cm absolute data is shown in Figure 7.

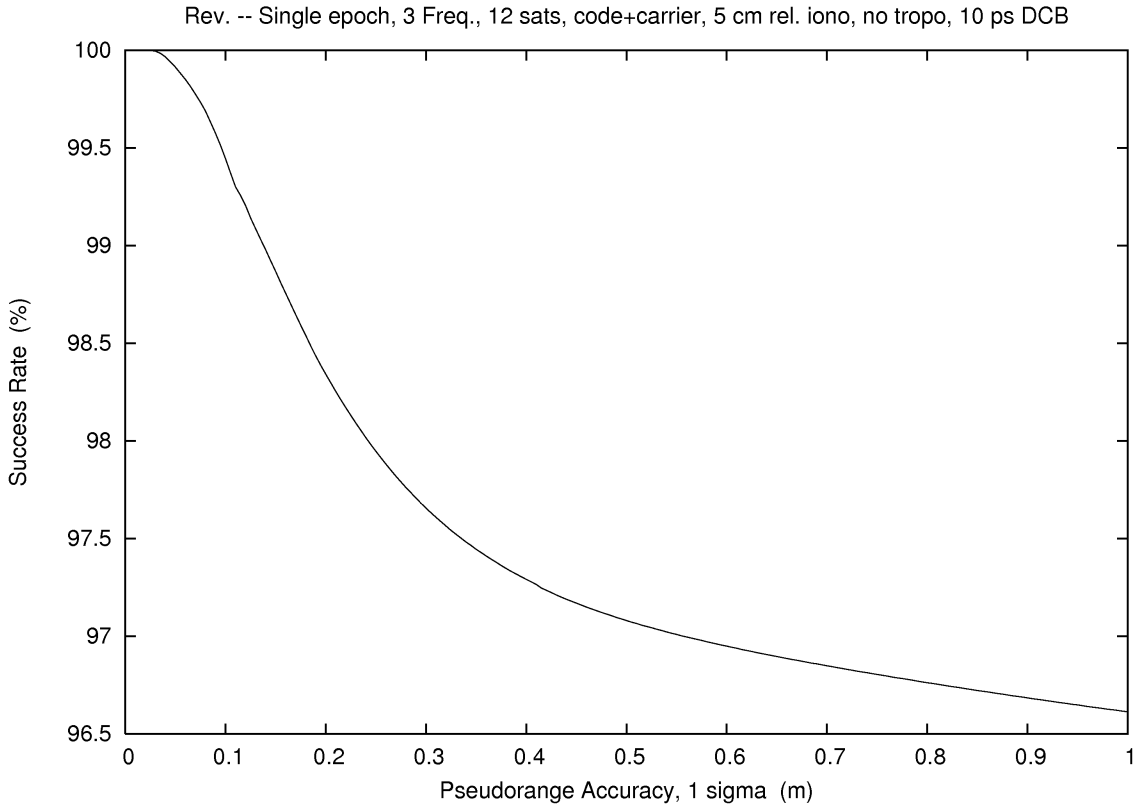

Fig 6. – Success Rate, L1/L2/L5, 5 cm Relative Ionosphere Model

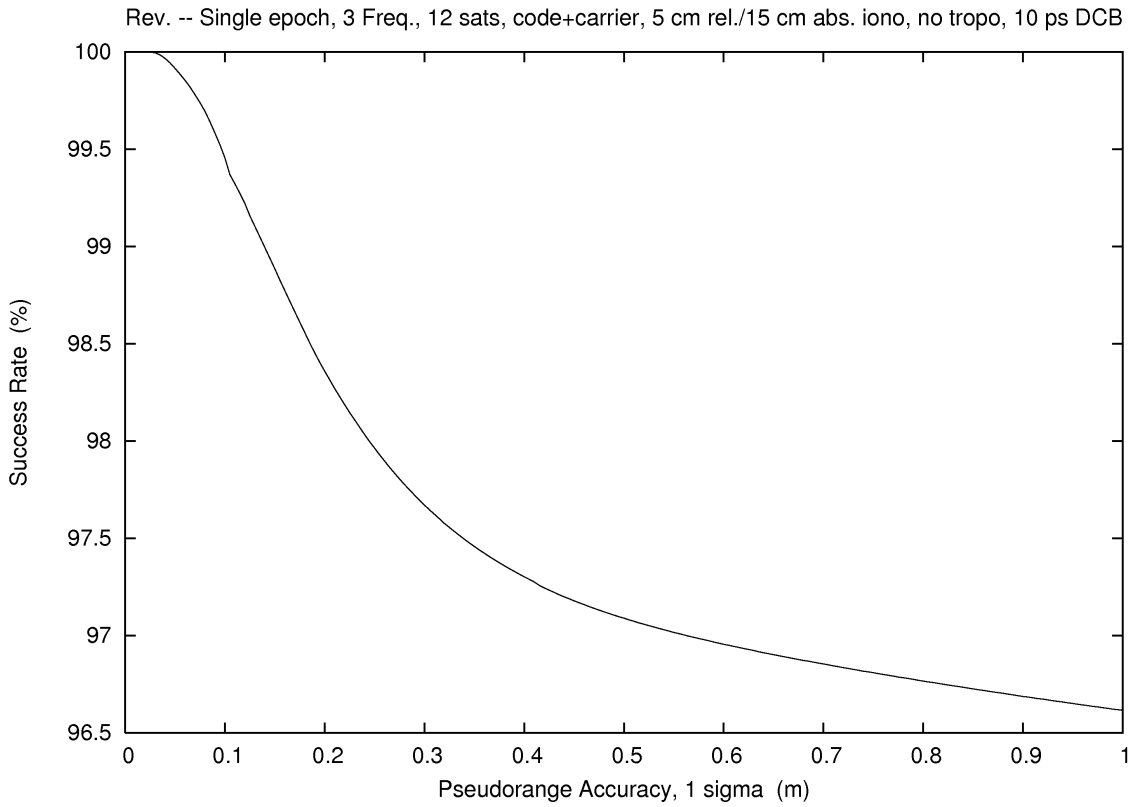

Fig 7. – Success Rate, L1/L2/L5, 5 cm Relative/15 cm Absolute Ionosphere Model

A major improvement in the success of resolving all 33 DD ambiguities is achieved by adding the relative ionosphere data. While the results are not as good as seen in Figure 3, recall that Figure 3 represents cases where either the ionosphere is perfectly known, or where the differential ionosphere effect is negligible. The addition of the absolute ionosphere weights of 15 cm RMS in Figure 7 gives a very tiny improvement, although it is not evident to the eye.

IONOSPHERE/TROPSPHERE ERROR SCENARIOS

This section completes the atmosphere propagation effects by considering troposphere delay. The troposphere is considered as modeled by means of NOAA models (for example: ftp://ddftp.fsl.noaa.gov/outgoing/gpsdist/zwdgrids). The residual troposphere error is assumed to be azimuthally symmetric. The residual zenith delay at each receiver is estimated, and a mapping function, M_D, dependent upon vertical angle, v, is used to relate the slant range delay to the zenith delay. Using L1 pseudorange as an example,

$$R_j^l = \rho_j^l + M_D(v)T_j + I_{ij}^{kl} + I_j^k + I_i^l - I_i^k + dt_j - dt^l \qquad (23)$$

where

T_i, T_j residual zenith tropospheric delay at receiver i or j (meters)
$M_D(v)$ Neill hydrostatic (dry) mapping function

The residual troposphere delay term is added to all pseudorange and carrier phase equations, where T_i is estimated for the base receiver, and T_j is estimated for the rover receiver. The complete set of models with the troposphere term is not given, but a tabulation of all the unknown parameters is provided in the Appendix.

In general practice one corrects for the dry troposphere effect and parameterizes the wet troposphere. But, with the availability of the NOAA models of dry and wet tropospheric delay, both elements should have very good corrections. It is assumed that the residual model error will be best mapped by the dominant source, the hydrostatic troposphere. Hence, the Neill hydrostatic mapping function, NMFH2.0, is chosen [17]. The success rate for resolving all 33 DD ambiguities while estimating residual troposphere error is shown in Figure 8.

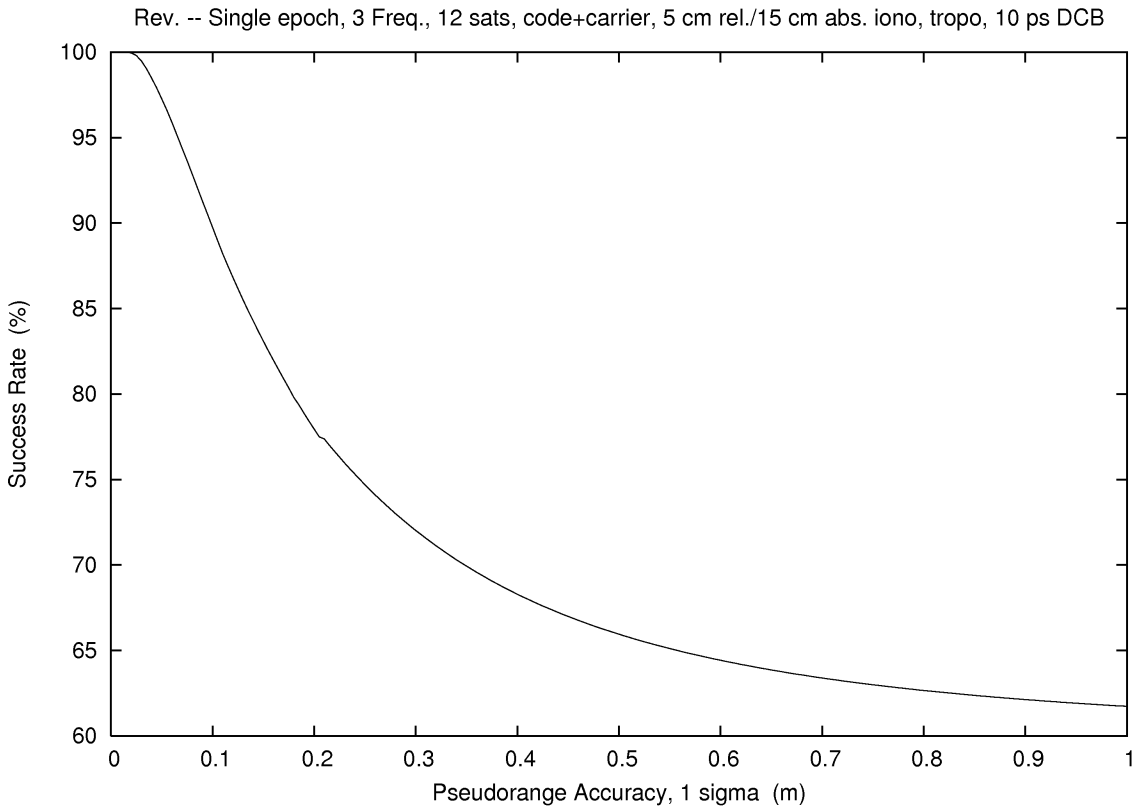

Fig 8. – Success Rate, L1/L2/L5, Weighted Ionosphere, Free Troposphere

The addition of the two residual tropospheric model terms has a significant effect on the ambiguity resolution success rate. Even so, some success is obtained if the pseudorange accuracy can be driven to about 20 cm.

Since the residual troposphere error estimation is performed in the context of *a priori* troposphere correction, we weight the troposphere terms based on the accuracy of the corrections. Referring to the formal accuracy in Figure 3 of [18], a 5 mm RMS zenith delay accuracy is adopted. Figure 9 shows the success rates when the 5 mm RMS is applied to the base receiver residual troposphere parameter, T_i.

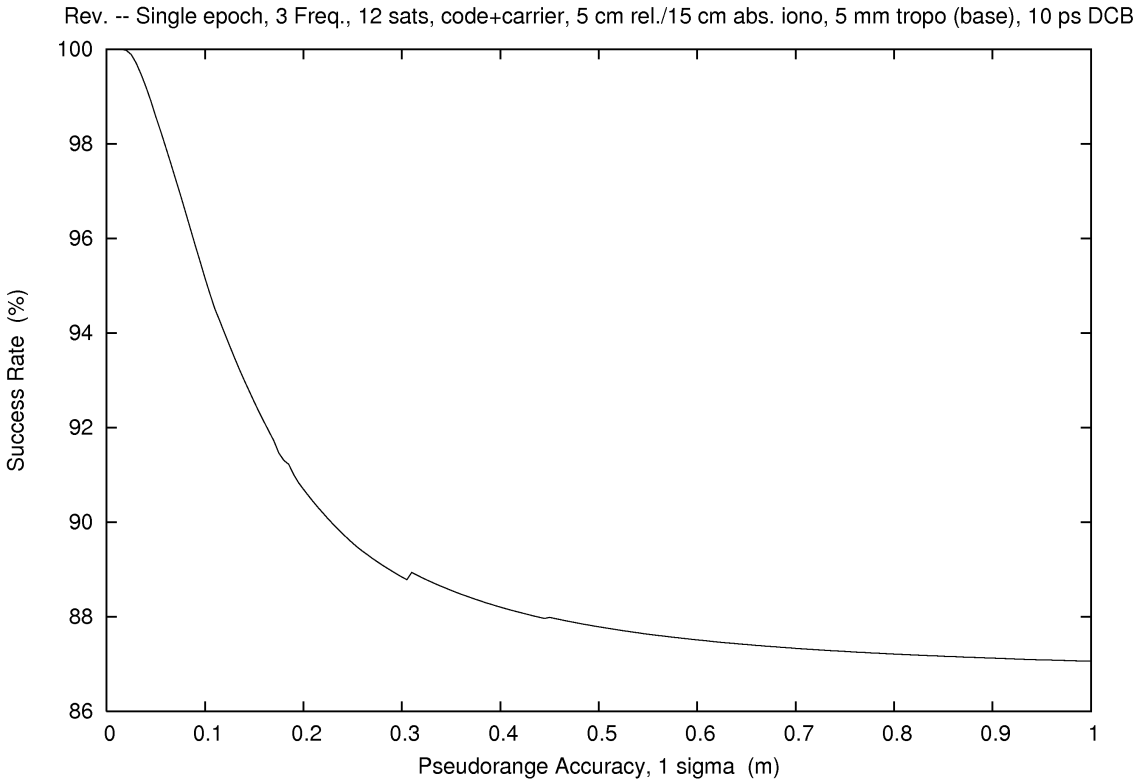

Fig 9. – Success Rate, L1/L2/L5, Weighted Ionosphere, 5 mm Base Troposphere

The success rate has considerable improvement, even when the weight is applied only to the base receiver. This would represent the case where the troposphere model has generally good performance, but where a differential troposphere effect needs to be unconstrained to get an effective solution.

Figure 10 shows the success rates when 5 mm RMS is applied to both the base and rover receiver residual troposphere parameters. This would be the expected success rate when the troposphere model is performing within its current formal error bounds.

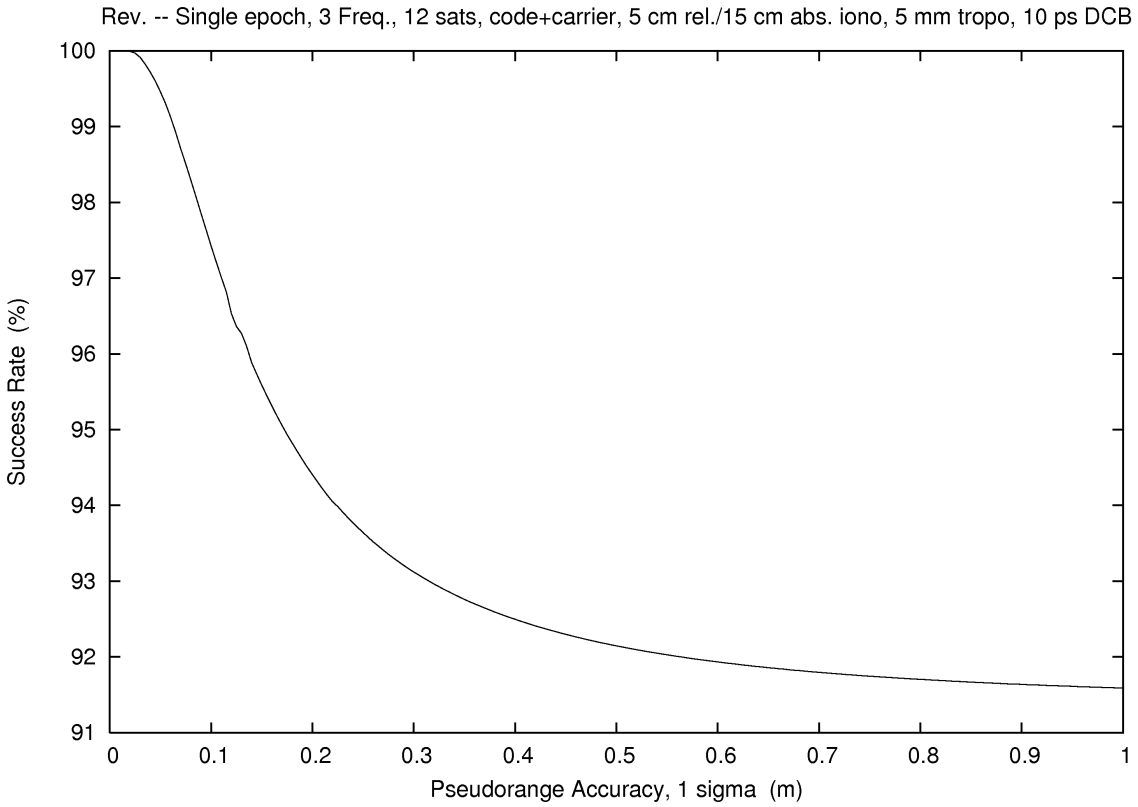

Fig 10. – Success Rate, L1/L2/L5, Weighted Ionosphere, 5 mm Base/Rover Troposphere

This last figure displays the influence of pseudorange accuracy when both tropospheric and ionospheric error sources are augmented by gridded data. It is seen that a very good success rate (95-97%) for single epoch solution is obtained with a 10 to 20 cm pseudorange RMS.

DISCUSSION

The objective for this paper is to explore additional factors in the modernization of GPS and the deployment of Galileo as they pertain to centimeter-level positioning. Numerous augmentation infrastructures could be envisioned. For example, a radiobeacon transmission of base receiver GNSS carrier phase data, NOAA atmospheric models, and DCB calibration elements through a system like HA-NDGPS [19] is possible.

The focus of this study, modernized pseudorange accuracy, is comprised partly of signal-in-space and partly of user equipment contributions. Atmospheric effects were modeled separately. Clock error would not seem to apply to the target accuracy, since both receiver and satellite clock error were estimated. Only those factors that would not be cancelled in a DD pseudorange measurement, such as receiver antenna multipath, would be considered in a notional pseudorange error budget.

These results could be extended in numerous ways. No real distinction is made between GPS and Galileo. The two constellations could be modeled with particular orbital planes and slot assignments. The exact L2 frequency of Galileo (E5b) could be used. Separate error budgets for carrier phase and pseudorange could be assigned to the two constellations. If orbital geometries have detailed modeling, then one should consider them around the globe and throughout the repeat cycle of the two systems.

An additional goal was to study the impact of supporting models. It was seen that DCB and atmospheric data improved the solutions. What has not been considered is the future synergy between GPS modernization, Galileo deployment, and likely improvement in these support models and calibration. Such a synergy will increase the success rates displayed here.

Other support data not studied here in detail are datum and error propagation effects of satellite clock and orbit data. If a study along the lines of this paper is conducted that includes these factors, then the boundary between relative and absolute (point) positioning will begin to blur. This could lead to future consideration of a hybridized solution method.

CONCLUSIONS

A simulation of single epoch ambiguity resolution success rate under varying levels of pseudorange accuracy is conducted with a hypothetical, 12 satellite in view, GNSS configuration. Short baselines scenarios, which neglect atmospheric errors, show uniformly high (> 97%) success rates of resolving all DD ambiguities. Long baseline scenarios, which include atmospheric error, show distinctly lower success. Adding weights that reflect the accuracy of DCB calibrations, ionosphere, and troposphere model data, greatly improves the success rates. When these factors are integrated into the models, single epoch ambiguity resolution success rates of 95 to 97% are obtained with a 10 to 20 cm pseudorange RMS. It may be concluded that increased pseudorange accuracy is an important goal in GPS modernization, and deserves additional study.

ACKNOWLEDGEMENTS

Thanks are given to the Mathematical Geodesy and Positioning Group of the Delft University of Technology for providing the LAMBDA software. Also, thanks are given to Dr. Dru Smith for inspiring this study. The author thanks Dr. Smith and an anonymous reviewer for their helpful suggestions.

APPENDIX

Table A-1 – Unknown Parameters, Full Model

Number of Unknowns (N--number of satellites)	Type
N-1	L1 integer DD carrier ambiguities
N-1	L2 integer DD carrier ambiguities
N-1	L5 integer DD carrier ambiguities
3	rover position (XYZ)
2	pseudorange receiver lumped bias (base and rover)
2	receiver L2/L1 DCB (base and rover)
2	receiver L5/L1 DCB (base and rover)
1	satellite L2/L1 DCB, pivot satellite
1	satellite L5/L1 DCB, pivot satellite
N-1	pseudorange satellite lumped bias, non-pivot
N-1	satellite L2/L1 DCB, non-pivot
N-1	satellite L5/L1 DCB, non-pivot
1	L1 float ambiguity, pivot satellite to base
1	L1 float ambiguity, pivot satellite to rover
N-1	L1 float ambiguity, non-pivot satellites to base
1	L2 float ambiguity, pivot satellite to base
1	L2 float ambiguity, pivot satellite to rover
N-1	L2 float ambiguity, non-pivot satellites to base
1	L5 float ambiguity, pivot satellite to base
1	L5 float ambiguity, pivot satellite to rover
N-1	L5 float ambiguity, non-pivot satellites to base
N-1	DD ionosphere
1	undifferenced iono, pivot satellite to base
1	undifferenced iono, pivot satellite to rover
N-1	undifferenced iono, non-pivot satellites to base
1	residual troposphere, base receiver
1	residual troposphere, rover receiver

REFERENCES

1. Verhagen, S., *Studying the Performance of Global Navigation Satellite Systems: A New Software Tool*, GPS World, Vol. 13, No. 6, June 2002, pp. 60-65.

2. Odijk, D., *Stochastic Modelling of the Ionosphere for Fast GPS Ambiguity Resolution*, Geodesy Beyond 2000: The Challenges of the First Decade, IAG General Assembly, Vol. 121, Birmingham UK, July 19-30, 1999, pp. 387-392.

3. Odijk, D., *Fast Precise GPS Positioning in the Presence of Ionospheric Delays*, Publications on Geodesy 52, Netherlands Geodetic Commission, Delft, Netherlands, November 2002.

4. Teunissen, P. J. G. and N. F. Jonkman, *Will Geometry-Free Full Ambiguity Resolution be Possible at All for Long Baselines*?, Proceedings of the ION 2001 National Technical Meeting, Long Beach, CA, January 22-24, 2001, pp. 271-280.

5. Crews, M., *GPS Modernization*, Presentations of the 44th Meeting of CGSIC, Long Beach, CA, September 20-21, 2004.

6. Taylor, J. and E. Barnes, *GPS Current Signal-in-Space Navigation Performance*, Proceedings of the ION 2005 National Technical Meeting, San Diego, CA, January 24-26, 2005.

7. Falcone, M., F. Amarillo, and E. Van Der Wenden, *Assessment of GALILEO Performance Based on the GALILEO System Test Bed Experimentation Results*, Institute of Navigation ION GNSS 2004, Long Beach, California, September 21-24, 2004.

8. Goad, C. C., *Precise Relative Position Determination Using Global Positioning System Carrier Phase Measurements in a Nondifference Mode*, in Proceedings of the First Symposium on Precise Positioning with the Global Positioning System, Positioning with GPS-1985, National Geodetic Survey, NOAA, Silver Spring, Maryland, 1985, pp. 347-356.

9. Teunissen, P. J. G., *Least-Squares Estimation of the Integer GPS Ambiguities*, Invited lecture, Sect IV, Theory and Methodology, IAG General Meeting, Beijing, August 1993.

10. Teunissen, P. J. G., P. J. de Jonge, C. C. J. M. Tiberius, *A New Way to Fix Carrier-Phase Ambiguities*, GPS World, Vol. 6, No. 4, April 1995, pp. 58-61.

11. Teunissen, P. J. G., P. J. de Jonge, C. C. J. M. Tiberius, *Performance of the LAMBDA Method for Fast GPS Ambiguity Resolution*, NAVIGATION, Journal of the Institute of Navigation, Vol. 44, No. 3, Fall 1997, pp. 373-383.

12. Joosten, P. and C. C. J. M. Tiberius, *Fixing the Ambiguities: Are You Sure They're Right*?, GPS World, Vol. 11, No. 5, May 2000, pp. 46-51.

13. Hein, G. W., J. Godet, J. Issler, J. Martin, P. Erhard, R. Lucas-Rodriguez, and T. Pratt, *Status of Galileo Frequency and Signal Design*, Institute of Navigation ION GPS 2002, Portland, Oregon, September 24-27, 2002.

14. Schaer, S., W. Gurtner and J. Feltens, *IONEX: The IONosphere Map Exchange Format Version 1*, February 25, 1998, Center for Orbit Determination in Europe (CODE), Astronomical Institute of the University of Berne (IAUB), Berne, Switzerland.

15. CODE, Center for Orbit Determination in Europe (CODE), web site and electronic products, http://www.aiub.unibe.ch/ionosphere/index.html.

16. Smith, D., *Ionospheric Monitoring Using NOAA's CORS Network*, Presentations of the 44th Meeting of CGSIC, Long Beach, CA, September 20-21, 2004

17. Niell, A. E., *Global Mapping Functions for the Atmospheric Delay at Radio Wavelengths*, Journal of Geophysical Research, Vol. 101, No. B2, February 10, 1996, pp. 3227-3246.

18. Gutman, S. I., S. R. Sahm, S. G. Benjamin, and T. L. Smith, *GPS Water Vapor Observation Errors*, Eighth Symposium on Integrated Observing and Assimilation Systems for Atmosphere, Oceans, and Land Surface (IOAS-AOLS), 84th American Meteorological Society Annual Meeting, Seattle, Washington, January 10-16, 2004.

19. Arnold, J., *High Accuracy Nationwide Differential Global Positioning System (HA-NDGPS) Broadcast*, Presentations of the 44th Meeting of CGSIC, Long Beach, CA, September 20-21, 2004

AUTHOR NOTES

This article was first published by The Institute of Navigation in the journal, NAVIGATION, Spring 2005, Volume 52, Number 1, pp.29-38. Typographical errors were corrected in equations 17 and 23. Reference is also made to Galileo frequency E5b.